**Supplemental Material**

**Table of Contents**

## 1. Supplemental Methods

### A. Patients and Genetic Screening

Initially, patient I-II-7 with tubulopathy and deafness was analyzed under the suspicion of EAST/SeSAME syndrome. Following the exclusion of pathogenic mutations in *KCNJ10*, *KCNJ16* was analyzed in a candidate gene approach. After the development of metabolic acidosis in this patient, a cohort of 53 patients (including patients from families B to F) with suspected renal tubular acidosis (RTA) was screened. Of these, 44 patients were tested by an NGS panel that included KCNJ10, 9 patients were tested by conventional Sanger sequencing. Patient E-II-1 was subjected to whole exome sequencing after exclusion of mutations in K*CNJ10*. Solely, patient G-II-1 with Gitelman-like renal phenotype was analyzed independently by whole exome sequencing after negative tubulopathy panel testing. A screening of a cohort of 11 patients with severe hypokalemia and suspected Bartter/Gitelman syndrome did not yield additional KCNJ16 mutations.

### B. Clinical exome sequencing and data analysis

DNA of patients D-II-2 and G-II-2 was extracted from peripheral blood samples and enriched with the Agilent SureSelectXT Human All Exon 50Mb Kit (Santa Clare, CA, USA). WES was performed using an Illumina Hiseq 2000TM sequencer (Copenhagen, Denmark). Following read alignment with BWA and variant calling with GATK, variants were annotated using an in-house developed program at the department of Genetics of the Radboud UMC. Criteria for variant pathogenicity followed the ACMG 2015 guidelines. In general, frequency of variants in

control populations (< 5% in dbSNP and <1% in an in-house database), nucleotide and amino acid conservation, inheritance pattern and the phenotype associated with the genes was combined to prioritize variants. The compound-heterozygous (D-II-2) and homozygous (G-II-2) *KCNJ16* variants were identified in open exome analysis *after* virtual gene panel analysis for renal disease.

Next-generation sequencing in patient D-II-1 was performed through Perkin Elmer (www.perkinelmer.com) and Illumina (www.illumina.com) as described previously [1]. Sequencing data were analyzed with an in-house pipeline, as well as Ingenuity variant analysis software (www.ingenuity.com). Identified mutations in *KCNJ16* were confirmed with Sanger sequencing.

**C. Microdissection of renal tubules**

Nephron segments were obtained from the kidneys of adult (8-10 week) male C57BL6J mice, briefly digested with type-2 collagenase, as previously described [2]. The glomeruli and tubules were isolated manually according to the morphological differences, before being lysed in RNA extraction buffer from RNAqueous® Total RNA Isolation Kit (Invitrogen, Carlsbad, CA). Quantitative reverse transcription polymerase chain reaction was performed on 5 pools of ~70 isolated renal tubules, obtained from 5 kidneys / 3 mice.

**D. RNA isolation and quantitative RT-PCR**

Total RNA was extracted from the mouse kidney segments with RNAqueousR kit (Applied Biosystems, Life Technologies). One µg of RNA was used to perform the reverse transcriptase reaction with iScript TM cDNA Synthesis Kit (Bio-Rad). Changes in mRNA levels of the target genes were determined by relative RT-qPCR with a CFX96TM Real-Time PCR Detection System

(Bio-Rad) using iQ TM SYBR Green Supermix (Bio-Rad). The analyses were performed in duplicate with 100nM of both sense and anti-sense primers in a final volume of 20µL using iQTM SYBR Green Supermix (Bio-Rad). Primers for segment-specific genes were designed using Primer3 as described [3]. PCR conditions were 95°C for 3 min followed by 40 cycles of 15 sec at 95°C, 30 sec at 60°C. The PCR products were sequenced with the BigDye terminator kit (Perkin Elmer Applied Biosystems) using ABI3100 capillary sequencer (Perkin Elmer Applied Biosystems). The efficiency of each set of primers was determined by dilution curves. The relative changes in targeted genes over Gapdh mRNA were calculated using the $2^{-\Delta\Delta Ct}$ formula.

**E. In situ hybridization**

Fluorescent multiplex in situ hybridization (RNAscope) assays (Advanced Cell Diagnostics, Hayward, CA) were used to visualize single RNA molecules per cell in 10 µm cryo-sections of wildtype mouse kidney fixed with 10% neutral buffered formalin. Kidney sections were incubated with Probe-C2 for *Kcnj16* (20ZZ probe targeting mouse *Kcnj16*, NM_001252207.1), Probe-C3 for *Umod* (20ZZ probe targeting mouse *Umod*, NM_009470.5), Probe-C1 for *Aqp1* (20ZZ probe targeting mouse *Aqp1*, NM_007472.2), and Probe-C1 for *Avpr2* (20ZZ probe targeting variants 1-3 of mouse *Avpr2*, NM_019404.2; NM_001276298.1; NM_001276299.1). Images were obtained with a confocal microscope SP8 (Leica Microsystems, Wetzlar, Germany).

**F. Patch clamp experiments in HEK293 cells**

Experiments were essentially performed as described previously [4]. HEK293T cells were transiently transfected with 0.025µg hKCNJ10-pIRES_CD8 plasmid. For hKCNJ16-HA-pIRES_CD8 or mutant hKCNJ16 variants containing plasmids, always 0.225 µg were used for

co-transfection with KCNJ10. The stoichiometric ratio of 1:10 was used to minimize homomeric KCNJ10 channel assembly. Measurements were performed one day after transfection of cells.

Cell-attached patch-clamp recordings were performed using an EPC-10 amplifier (HEKA) and the PatchMaster software. The patch pipette solution was composed of 95 mM K-gluconate, 30 mM KCl, 4.8 mM $Na_2HPO_4$ , 1.2 mM $NaH_2PO_4$, 5 mM Glucose, 1 mM EGTA, 2 mM Na-ATP, 2.38 mM $MgCl_2$ and 0.726 mM $CaCl_2$ (pH 7.2). The bath solution contained 145 mM NaCl, 5 mM Hepes, 1.6 mM $K_2HPO_4$, 0.4 mM $KH_2PO_4$, 5mM Glucose, 1 mM $MgCl_2$ and 1.3 mM $CaCl_2$ (pH 7.4). The liquid junction potential was 10 mV and was corrected by the PatchMaster software. All measurements were carried out at room temperature.

**2. Supplemental Results**

**A. Audiograms**

Figure S1: Binaural summation curve in the free sound field elicited with different acoustic stimuli in individual A-II-7 at the age of 10 months. ○ = warble, □ = narrow band noise

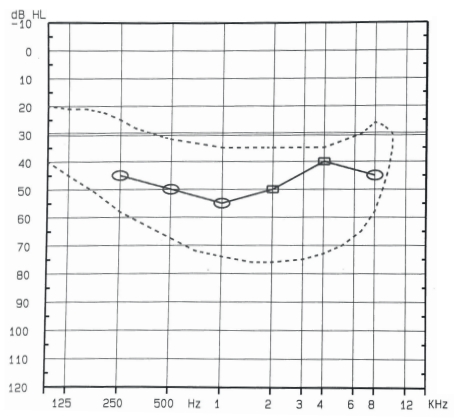

Figure S2: Bilateral audiograms of individual B-II-1 at 9 years of age. Air conduction, ○ = right ear, X = left ear; Bone conduction, < = right ear, > = left ear.

Right ear Left ear

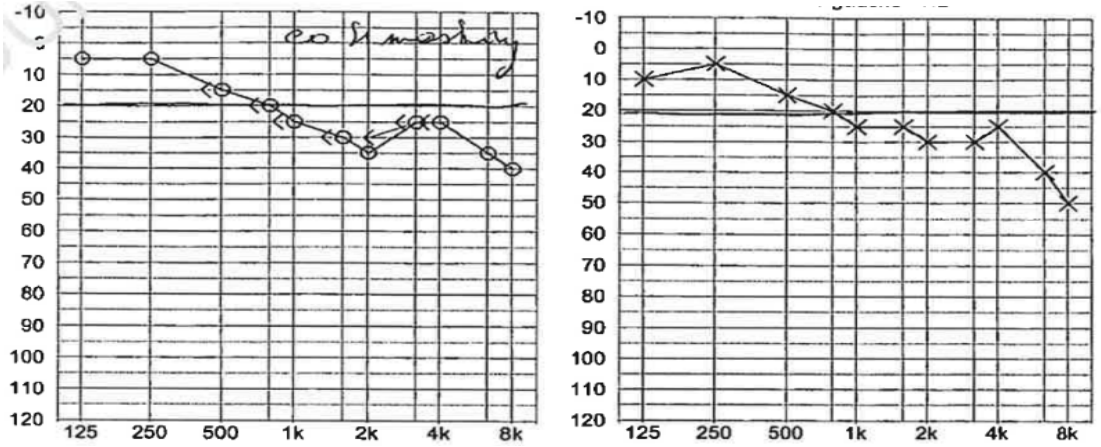


Figure S3: Bilateral audiograms of individual D-II-2 at 5 years of age (without hearing aids).

Right ear Left ear

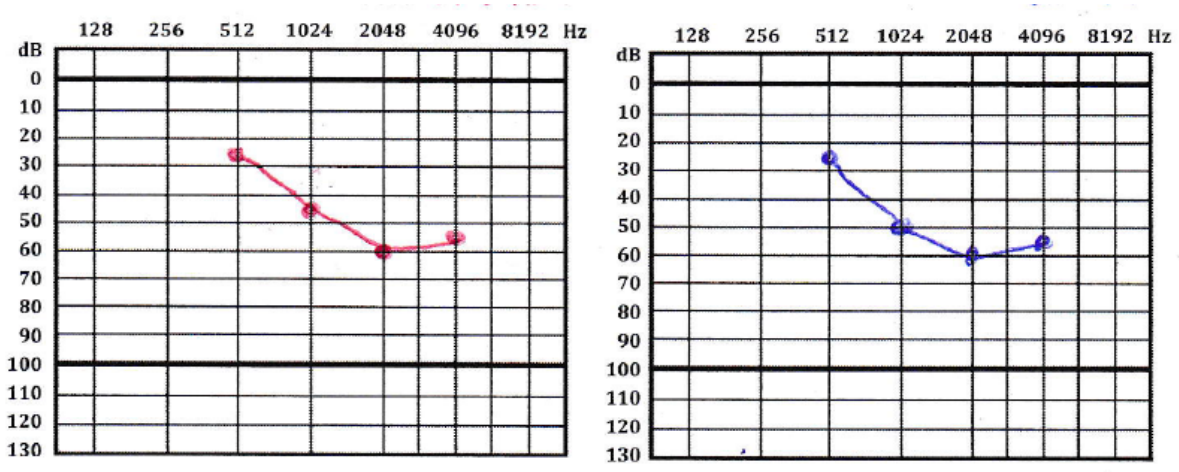

Figure S4: Bilateral audiograms of individual G-II-2 at adult age. Air conduction, ○ = right ear, X = left ear; Bone conduction, < = right ear, > = left ear.

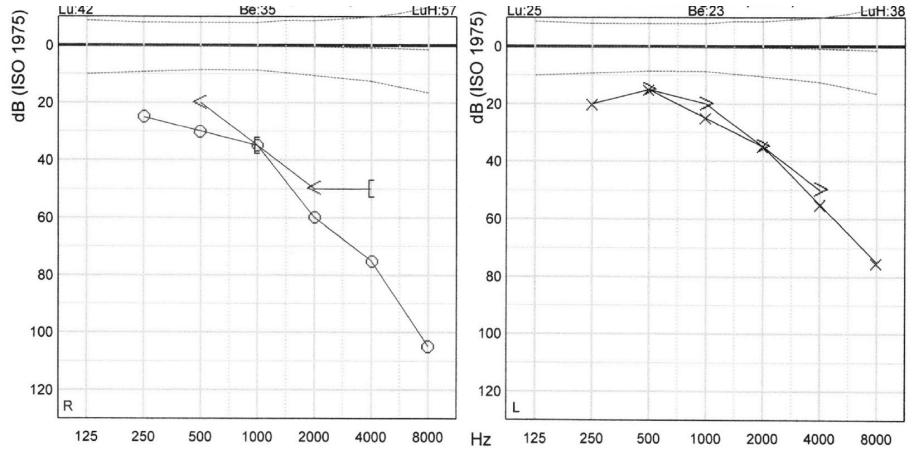

**B. Figure S5: On-cell patch-clamp experiments after co-expression of wildtype and mutant KCNJ16 and KCNJ10 in HEK293 cells.**

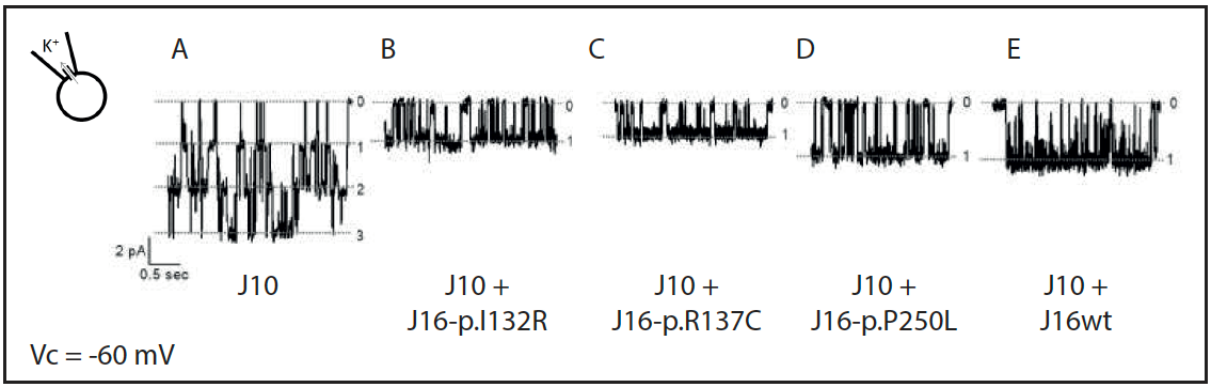


Single-channel properties of KCNJ10 alone and co-expressed with wildtype and mutant KCNJ16 on transfected HEK293 cells in cell-attached configuration at clamped voltage (Vc) = -60 mV. (A) Cells transfected with KCNJ10 channels showed clear single-channel levels and a high open probability (70–80%)(3 channel complexes in the patch). (B-E) Co-transfection with mutant (p.I132R, p.R137C, and p.P250L) and wildtype KCNJ16. Co-transfection with wildtype KCNJ16 (E) results in a significant increase in current amplitude without significant change in the mean open probability. Co-expression of C-terminal mutant KCNJ16-p.P250L with KCNJ10 resulted in a current amplitude comparable to wildtype KCNJ16 putatively reflecting a heteromeric channel complex at the plasma membrane. In contrast, after co-expression of pore mutants KCNJ16-p.I132R and -p.R137C, single-channel current amplitudes comparable to that obtained after expression of KCNJ10 alone were recorded suggesting a remaining homomeric KCNJ10 channel complex at the plasma membrane.

**C. Supplemental Table S1**

| **Patient** | A-II-7 | B-II-1 | B-II-2 | C-II-1 | D-II-2 | E-II-1 | F-II-1 | G-II-2 |
|---|---|---|---|---|---|---|---|---|
| **Sanger Seq *KCNJ10*** | p.R137C homozygous | p.R137C + p.R176* | p.R137C + p.R176* | p.I132R + p.R176* | used for confirmation of NGS result | used for confirmation of NGS result | p.G135A + p.R176* | used for confirmation of NGS result |
| **Sanger Seq *KCNJ10*** | negative | n.d. | n.d. | n.d. | n.d. | n.d. | negative | n.d. |
| **Tubulopathy Panel (incl. KCNJ10)** | n.d. | n.d. | n.d. | negative | negative | negative | n.d. | negative |
| **Whole Exome** | n.d. | n.d. | n.d. | n.d. | KCNJ16-p.I132R + p.R176* | KCNJ16-p.I132R + p.P250L | n.d. | KCNJ16 p.T64I homozygous |
| **Segregation analysis (parents)** | both parents heterozygous | p.R137C from mother, p.R176* from father | p.R137C from mother, p.R176* from father | p.I132R from father, p.R176* from mother | n.d. | p.I132R from father, p.P250L from mother | n.d. | both parents heterozygous |

**Supplemental Table S2: Primer sequences**

| Gene name | Forward primer (5'-3') | Reverse primer (5'-3') | PCR products (bps) | Efficiency |
|---|---|---|---|---|
| *Gapdh* | TGCACCACCAACTGCTTAGC | GGATGCAGGGATGATGTTCT | 176 | 1.04 ± 0.03 |
| *Npsh2* | GTCTAGCCCATGTGTCCAAA | CCACTTTGATGCCCCAAATA | 162 | 1.03 ± 0.03 |
| *Slc12a3* | CATGGTCTCCTTTGCCAACT | TGCCAAAGAAGCTACCATCA | 148 | 1.01 ± 0.03 |
| *Slc12a1* | CCGTGGCCTACATAGGTGTT | GGCTCGTGTTGACATCTTGA | 154 | 0.99 ± 0.04 |
| *Aqp2* | TCACTGGGTCTTCTGGATCG | CGTTCCTCCCAGTCAGTGT | 147 | 1.03 ± 0.04 |
| *Slc5a2* | TTGGGCATCACCATGATTTA | GCTCCCAGGTATTTGTCGAA | 164 | 1.01 ± 0.03 |
| *Slc38a3* | GTTATCTTCGCCCCCAACAT | TGGGCATGATTCGGAAGTAG | 109 | 0.99 ± 0.02 |
| *Kcnj16* | ATCCTCCAGAGCATGCCATC | TACGAACATATGGCGCCACT | 167 | 1.02 ± 0.03 |
| *Kcnj15* | CGTGTTGGATGAGACAAGCC | GGAGAGAGAAACCACAGGCA | 187 | 1.02 ± 0.02 |
| *Kcnj10* | CCTGAGTGGGACAGTGGAGT | TGGTCGAAAAGGCTGAAGTC | 150 | 1.01 ± 0.03 |

## 3. References


1. Cabezas, O.R., Flanagan, S.E., Stanescu, H., García-Martínez, E., Caswell, R., Lango-Allen, H., Antón-Gamero, M., Argente, J., Bussell, A.M., Brandli, A., et al. (2017). Polycystic Kidney Disease with Hyperinsulinemic Hypoglycemia Caused by a Promoter Mutation in Phosphomannomutase 2. J Am Soc Nephrol 28, 2529-2539.

2. Glaudemans, B., Terryn, S., Gölz, N., Brunati, M., Cattaneo, A., Bachi, A., Al-Qusairi, L., Ziegler, U., Staub, O., Rampoldi, L., et al. (2014). A primary culture system of mouse thick ascending limb cells with preserved function and uromodulin processing. Pflugers Arch 466, 343-356.

3. Tokonami, N., Takata, T., Beyeler, J., Ehrbar, I., Yoshifuji, A., Christensen, E.I., Loffing, J., Devuyst, O., and Olinger, E.G. (2018). Uromodulin is expressed in the distal convoluted tubule, where it is critical for regulation of the sodium chloride cotransporter NCC. Kidney Int 94, 701-715.

4. Reichold, M., Zdebik, A.A., Lieberer, E., Rapedius, M., Schmidt, K., Bandulik, S., Sterner, C., Tegtmeier, I., Penton, D., Baukrowitz, T., et al. (2010). KCNJ10 gene mutations causing EAST syndrome (epilepsy, ataxia, sensorineural deafness, and tubulopathy) disrupt channel function. Proc Natl Acad Sci U S A 107, 14490-14495.